Bioorganic & Medicinal Chemistry Letters 21 (2011) 4054–4058

Contents lists available at ScienceDirect

Bioorganic & Medicinal Chemistry Letters

journal homepage: www.elsevier.com/locate/bmcl

Structure-based design of thienobenzoxepin inhibitors of PI3-kinase

Steven T. Staben [a,*], Michael Siu [a], Richard Goldsmith [a], Alan G. Olivero [a], Steven Do [a], Daniel J. Burdick [a], Timothy P. Heffron [a], Jenna Dotson [a], Daniel P. Sutherlin [a], Bing-Yan Zhu [a], Vickie Tsui [a], Hoa Le [d], Leslie Lee [b], John Lesnick [c], Cristina Lewis [c], Jeremy M. Murray [e], Jim Nonomiya [c], Jodie Pang [d], Wei Wei Prior [b], Laurent Salphati [d], Lionel Rouge [e], Deepak Sampath [b], Steve Sideris [c], Christian Wiesmann [e], Ping Wu [e]

[a] Discovery Chemistry, Genentech, Inc., 1 DNA Way, South San Francisco, CA 94080, USA
[b] Small Molecule Translational Oncology, Genentech, Inc., 1 DNA Way, South San Francisco, CA 94080, USA
[c] Biochemical Pharmacology, Genentech, Inc., 1 DNA Way, South San Francisco, CA 94080, USA
[d] Drug Metabolism and Pharmacokinetics, Genentech, Inc., 1 DNA Way, South San Francisco, CA 94080, USA
[e] Structural Biology, Genentech, Inc., 1 DNA Way, South San Francisco, CA 94080, USA

ARTICLE INFO

Article history:
Received 5 March 2011
Revised 22 April 2011
Accepted 26 April 2011
Available online 13 May 2011

Keywords:
Structure-based design
PI3-kinase

ABSTRACT

Starting from thienobenzopyran HTS hit **1**, co-crystallization, molecular modeling and metabolic analysis were used to design potent and metabolically stable inhibitors of PI3-kinase. Compound **15** demonstrated PI3K pathway suppression in a mouse MCF7 xenograft model.

Increased signaling resulting from somatic mutation of the p110α subunit of PI3K and the lipid phosphatase PTEN provides evidence for the importance of the PI3K signalling pathway in a variety of human cancers.[1] Previous reports from our group have detailed the optimization of 4-morpholinothienopyrimidine PI3-kinase inhibitors including GNE-493,[2] GNE-477,[3] and GDC-0941[4] (currently in clinical studies). Our continued effort toward the discovery and development of inhibitors of the PI3K pathway for oncology applications led to the identification of benzopyran **1** from a high-throughput screen measuring single point inhibition of PI3Kα (Fig. 1, confirmed PI3Kα IC_{50} = 0.254 μM).[5] Although a poor starting point from the standpoint of potency relative to physicochemical properties (*c* Log *P* = 4.1, LE = 0.39, LipE = 2.5, MW = 356),[6] structural novelty of **1** made it a good candidate for further optimization.

A positional scan of aryl-substituents on the aniline amide revealed the importance of *o*-halogens for inhibitory activity (Table 1). Co-crystallization of **1f** in PI3Kγ suggested the ortho-halogen is located in a hydrophobic pocket defined by Ile831, Ile879 and Lys833 (Fig. 2).[7] It also indicated that the *N*-methyl aniline amide bound in a cis-fashion.[8] Analogs in which the 2-haloaryl ring was replaced with branched alkyl substituents (e.g., **2** and **3**) were significantly less potent, perhaps because conformational preference did not bias filling this hydrophobic pocket.

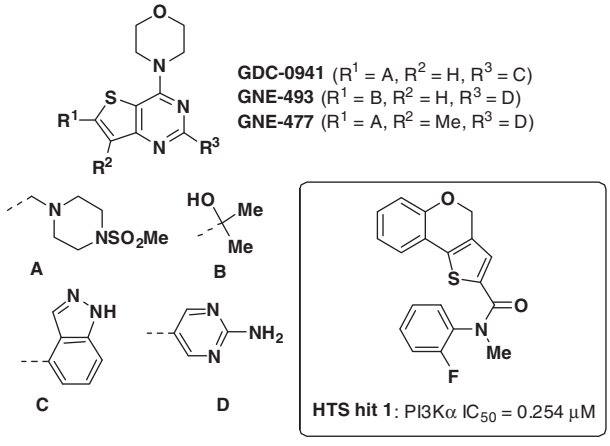

Figure 1. Previously disclosed thienopyrimidine inhibitors of PI3-Kinase from Genentech and thienobenzopyran HTS hit **1**.

This crystal structure also provided additional paths for potency improvement. The amide carbonyl of **1f** (Fig. 2) is positioned within water mediated H-bond distance to Tyr867 while the benzopyran oxygen forms a key, but suboptimal, H-bond with the hinge residue (3.6 Å). We anticipated that pyran ring-expansion would provide an improved interaction with the hinge as well as remove

* Corresponding author.
E-mail address: stevents@gene.com (S.T. Staben).

0960-894X/$ - see front matter © 2011 Elsevier Ltd. All rights reserved.
doi:10.1016/j.bmcl.2011.04.124

Table 1
Effect of amide substitution on P13α[a] IC_{50}

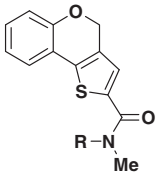

Compound	R	PI3Kα IC_{50} (μM)
1a	2-F-C_6H_4	0.254
1b	3-F-C_6H_4	~1.0
1c	4-F-C_6H_4	~1.0
1d	2-Me–C_6H_4	0.699
1e	2-OMe–C_6H_4	0.673
1f	2-Cl–C_6H_4	0.108
1g	2-Pyridyl	>10
2	^{i}Pr	5.2
3	^{i}Bu	17

[a] See Ref. 5 for a description of the assay conditions.

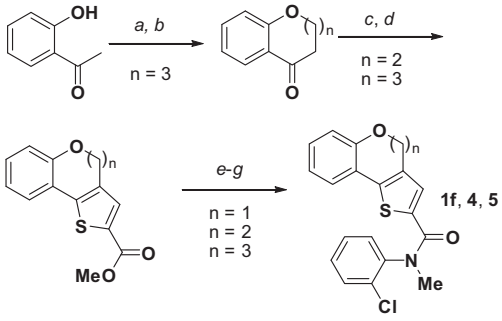

	n	PI3Kα IC_{50} (μM)	cLogP	LipE
1f	1	0.108	4.6	2.4
4	2	0.024	4.6	3
5	3	>10	5.1	–

Figure 3. Synthesis and biochemical potency of ring-expanded analogs.[9] (a) base, $BrCH_2CH_2Br$; (b) NaH; (c) $POCl_3$, DMF; (d) $HSCH_2CO_2Me$, DMF; (e) LiOH, THF/H_2O; (f) $SOCl_2$; (e) 2-Cl–N–Me–aniline, DIPEA, CH_2Cl_2. See Ref. 5 for a description of the assay conditions.

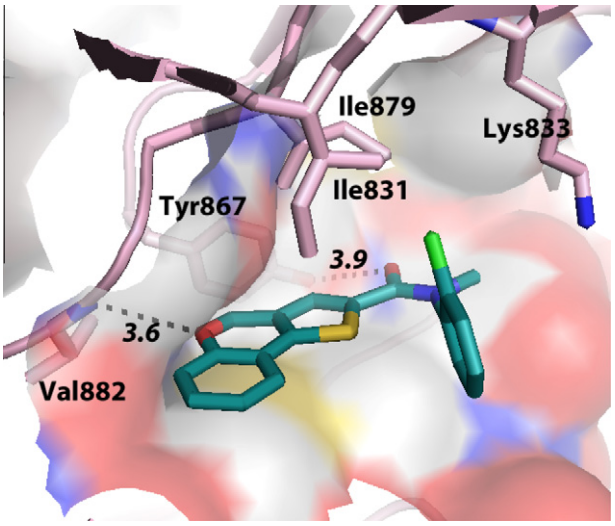

Figure 2. X-ray structure of **1f** soaked into PI3Kγ (PDB 3R7Q).

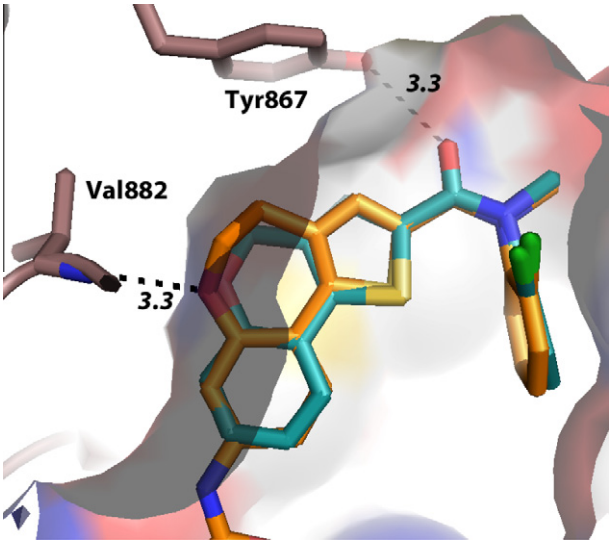

Figure 4. Overlay of X-ray structures of benzoxepin **6** (orange) and benzopyran **1f** (blue) in PI3Kγ (PDB 3R7R). Solvent exposed region omitted for clarity.

a benzylic ether methylene unit that could be prone to metabolic oxidation. The synthesis of representative benzopyran and ring-expanded analogs is presented in Figure 3. Alkylation of 2-hydroxyacetophenone with dibromoethane followed by sodium hydride promoted cyclization gave the benzoxocanone. A two step thiophene synthesis proceeding through the β-chloroenal gave a thieno-benzoxepin ($n = 2$) and thienobenzoxocane ($n = 3$). Amide bond formation was accomplished through intermediacy of acid chlorides to give final compounds **1f**, **4** and **5**.

Although benzoxocane **5** displayed little inhibition of PI3Kα, benzoxepin **4** was ~5-fold more potent than benzopyran **1f**.[10] This potency difference was consistent across a comparison of direct benzopyran/benzoxepin analogs. Notably, this change is calculated to be lipophilicity neutral, and therefore provides an improvement in lipophilic efficiency (LipE). Overlay of crystal structures of **1f** and **6** (vide infra) in PI3Kγ (Fig. 4) shows a shorter hydrogen bond and better angle to hinge-residue Val882. Improved occupancy of the binding pocket by an extra methylene unit could also be responsible for the potency increase against the PI3K isoforms.

Unfortunately, benzoxepin **4** was cleared at a rate greater than hepatic blood following intravenous administration to rat (Cl_p = 60 mL/min/kg). Our strategy became potency improvement with concomitant decreasing lipophilicity (progressive design driven by improving LipE).[11] We hypothesized that judicious substitution at the 8-position of the benzoxepin would improve potency and decrease lipophilicity while simultaneously hindering possible sites of metabolism.

Notably, improved potency against PI3Kα was achieved with *N*-acyl, *N*-carbamoyl, carbamide, and 4-pyrazolyl substitution (**6**–**9**, **11** in Table 2). Tertiary amides, that is, **10**, were less tolerated and generally were considerably less potent. Unfortunately, these lipophilicity-reducing modifications did not substantially improve clearance in rat.

We hypothesized amide hydrolysis, para-oxidation, or demethylation of the electron-rich *N*-methyl-aniline in these analogs might be responsible for the continually observed high clearance.[12] A metabolite ID experiment in human hepatocytes for **9** indeed identified significant hydrolysis of the aniline amide as well as an

Table 2
Benzoxepin 8- and 4-anilino substitution alters potency and clearance

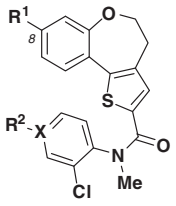

Compound	R^1	R^2	PI3Kα K_i (nM)	Prolif. MCF7.1 IC_{50} (μM)	Rat Cl_p (mL/min/kg)	Mouse Cl_p (mL/min/kg)	*c* Log *P*	LipE
4	H	H	16.3	2.9	60	ND	4.6	3.19
6		H	1.8	0.807	72	ND	3.9	4.84
7	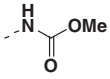	H	1.5	0.678	44	ND	4.5	4.32
8		H	1.2	6.2	89	ND	3.5	5.42
9		H	2.5	1.1	ND	ND	3.8	4.80
10	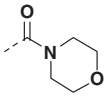	H	31	>30	ND	ND	3.3	4.21
11		H	0.6	12	ND	ND	4.9	4.32
12[a]	H	—	473	ND	23	ND	3.5	2.82
13[a]		—	65	3.3	ND	ND	3.7	3.49
14			2.5	0.719	28	24	3	5.60
15			3.7	0.303	36	15	2.7	5.73

X = C unless otherwise noted. [a] X = N. ND = not determined. Clearance values obtained from a discrete iv dose of 1 mg/kg or a cassette iv dose of 0.25 mg/kg. See Ref. 5 for a description of the assay conditions.

oxidative metabolite resulting from de-methylation, aromatic oxidation and glucoronindation of the aniline.[13] We projected that steric and electronic modification of the aniline, reducing lipophilicity while blocking para-oxidation, would not only decrease clearance but eliminate generation of these potentially toxic and reactive species.[14] Accordingly we synthesized **12** (*c* log *P* = 3.5), with a 4-aminopyridine replacement for the aniline. As hypothesized, **12** did display decreased clearance in rat (23 mL/min/kg), although lacked potency against PI3Kα which could not be sufficiently recovered with the most potent 8-substitution (i.e., **13**). We next examined substitution on the aniline ring with electron-withdrawing polar amide functionality (**14**, **15** Table 2). Gratifyingly, potency was maintained while lipophilicity was reduced (lipE **15** = 5.73) and a corresponding decrease in rodent clearance was observed. Interestingly, both the position and identity of the aniline substituent affected rodent clearance (Fig. 5). For example, transposition of the amide to the 5-position or replacement of the amide with a halide did not improve metabolic stability (**16**, **17**).

Interestingly, consistent decreased clearance with para-amide substitution could be seen in vivo over a broad range of benzoxepin inhibitors (Fig. 6). In addition to decreasing total clearance, the decreased lipophilicity with this substitution pattern (*c* log *P* = 2.7 for **15**, vs 3.8 for **9** and 4.6 for **4**) is likely responsible for a decreased cellular/enzymatic potency shift observed with these analogs (Table 2).

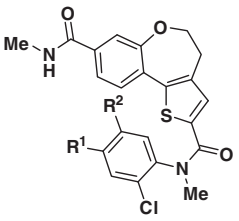

15, R^1 = $CONMe_2$, R^2 = H
16, R^1 = F, R^2 = H
17, R^1 = H, R^2 = $CONMe_2$

compound	clogP	Rat Cl_p (mL/min/kg)	Mouse Cl_p (mL/min/kg)
15	2.7	36	15
16	4.0	153	182
17	2.7	66	55

Figure 5. Identity and position of aniline substitution affects rodent clearance. Clearance values obtained from a discrete iv dose of 1 mg/kg or a cassette iv dose of 0.25 mg/kg.

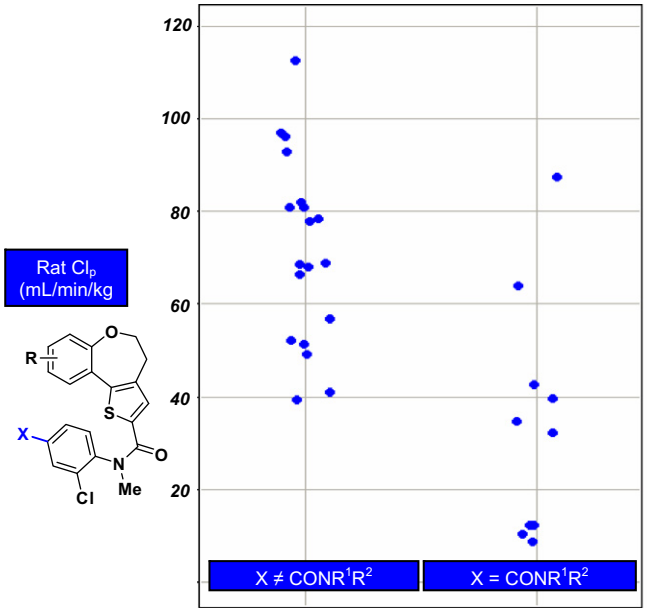

Figure 6. Substructure versus Rat Clp. Rat Clp was measured by iv dose between 0.25 and 1 mg/kg solution. Some values are determined by cassette dosing. Compound **16** (Clp = 153 mL/min/kg) omitted for clarity.

in vitro profile for **15**:

PI3Kα IC_{50}:	4.6 nM
PI3Kβ IC_{50}:	60 nM
PI3Kδ IC_{50}:	1.7 nM
PI3Kγ IC_{50}:	5.0 nM
mTOR IC_{50}:	530 nM
pAKT (PC3, S473):	310 nM
Prolif EC_{50} (PC3):	550 nM
Prolif EC_{50} (MCF7):	256 nM
ppb (%, H/R/M/D/C):	97/97/98/93/91

PK profile for **15**

species	Cl_p (mL/min/kg)	F%	dose, formulation	AUC (μM h)
rat	36	50	100 mg/kg, 60% PEG	39
mouse	15	28	100 mg/kg, MCT	330
dog	5	120	2 mg/kg, 60% PEG	17
cyno	10	--	--	--

Figure 7. In vitro and pharmacokinetic profile for **15** (GNE-614).

Compound **15** (GNE-614) was selected for further profiling based on its acceptable cellular potency and in vitro metabolic stability. This inhibitor was active against all class I PI3-kinase isoforms, yet relatively inactive against mTOR (Fig. 7). Compound **15** displayed low to moderate clearance across species and moderate to high bioavailability of suspension and solution oral doses. A single dose PK/PD in nude mice bearing an MCF7-neo/HER2 tumor xenograft demonstrated prolonged suppression of PI3K pathway markers including pAKT, pPRAS40 and pS6RP (Fig. 8) comparable to an equivalent dose of the clinical PI3-kinase inhibitor GDC-0941 at a 6-h timepoint.[15]

In summary, structure-based design was used to optimize benzopyran HTS hit **1** to potent and metabolically stable **15**. Importantly, **15** displayed significant suppression of PI3K-pathway markers in vivo. Disappointingly, **15** was identified as being a potent inhibitor of DNA-PK (IC_{50} = 6 nM). Future work within this series focused on improving bioavailability, removal of perceived structural liabilities, and decreasing potency against the DNA-PK counter-target. The results of these efforts will be disclosed in future publications. These inhibitors also presented a novel vector for exploring selectivity over PI3Kβ.[16]

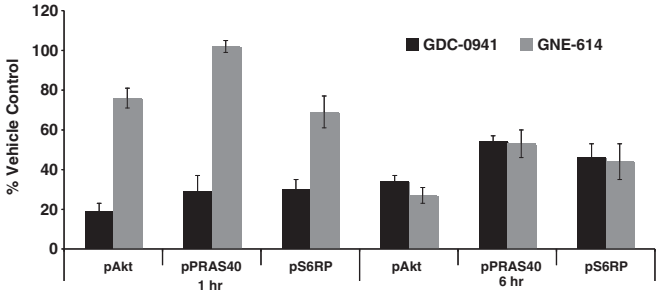

Figure 8. Comparison oral single dose PK/PD of **15** (GNE-614) and GDC-0941 at 50 mg/kg. Compound **15** shows significant pathway suppression in mice bearing MCF7-neo/HER2 tumor xenografts indicated as pAKT, pPRAS40, pS6RP levels relative to vehicle controls. At one hour $[\mathbf{15}]_{plasma}$ = 7.38 μM, $[\mathbf{GDC\text{-}0941}]_{plasma}$ = 6.72 μM, $[\mathbf{15}]_{tumor}$ = 1.08 μM, $[\mathbf{GDC\text{-}0941}]_{tumor}$ = 2.83 μM; at 6 h $[\mathbf{15}]_{plasma}$ = 11.10 μM, $[\mathbf{GDC\text{-}0941}]_{plasma}$ = 4.50 μM, $[\mathbf{15}]_{tumor}$ = 2.24 μM, $[\mathbf{GDC\text{-}0941}]_{tumor}$ = 1.34 μM.[14]

References and notes

1. (a) Shayesteh, L.; Kuo, W. L.; Baldocchi, R.; Godfrey, T.; Collins, C.; Pinkel, D.; Powell, B.; Mills, G. B.; Gray, J. W. *Nat. Genet.* **1999**, *21*, 99; (b) Samuels, Y.; Wang, Z.; Bardelli, A.; Silliman, N.; Ptak, J.; Szabo, S.; Yan, H.; Gazdar, A.; Powell, S. M.; Riggins, G. J.; Willson, J. K.; Markowitz, S.; Kinzler, K. W.; Vogelstein, B.; Velculescu, V. E. *Science* **2004**, *30*, 554; (c) Parsons, D. W.; Wang, T. L.; Samuels, Y.; Bardelli, A.; Cummins, J. M.; DeLong, L.; Silliman, N.; Ptak, J.; Szabo, S.; Willson, J. K.; Markowitz, S.; Kinzler, K. W.; Vogelstein, B.; Lengauer, C.; Velculescu, V. E. *Nature* **2005**, *436*, 792; (d) Chalhoub, N.; Baker, S. J. *Annu. Rev. Pathol. Mech. Dis.* **2009**, *4*, 127; (e) Hennessy, B. T.; Smith, D. L.; Ram, P. T.; Lu, Y.; Mills, G. B. *Nat. Rev. Drug Disc.* **2005**, *4*, 98; (f) Wee, S.; Lengauer, C.; Wiederschain, D. *Curr. Opin. Oncol.* **2008**, *20*, 77; (g) Marone, R.; Cmiljanovic, V.; Giese, B.; Wymann, M. P. *Biochim. Biophys. Acta* **2008**, *111*, 159; (h) Yap, T. A.; Garrett, M. D.; Walton, M. I.; Raynaud, F.; de Bono, J. S.; Workman, P. *Curr. Opin. Pharmacol.* **2008**, *8*, 393; (i) Crabbe, T.; Welham, M. J.; Ward, S. G. *Trends Biochem. Sci.* **2007**, *32*, 460.
2. Sutherlin, D. P.; Sampath, D.; Berry, M.; Castanedo, G.; Chang, Z.; Chuckowree, I.; Dotson, J.; Folkes, A.; Friedman, L.; Goldsmith, R.; Heffron, T.; Lee, L.; Lesnick, J.; Lewis, C.; Mathieu, S.; Nonomiya, J.; Olivero, A.; Pang, J.; Prior, W. W.; Salphati, L.; Sideris, S.; Tian, Q.; Tsui, V.; Wan, N. C.; Wang, S.; Wiesmann, C.; Wong, S.; Zhu, B.-Y. *J. Med. Chem.* **2010**, *53*, 1086.
3. Heffron, T. P.; Berry, M.; Castanedo, G.; Chang, C.; Chuckowree, I.; Dotson, J.; Folkes, A.; Gunzner, J.; Lesnick, J. D.; Lewis, C.; Mathieu, S.; Nonomiya, J.; Olivero, A.; Pang, J.; Peterson, D.; Salphati, L.; Sampath, D.; Sideris, S.; Sutherlin, D. P.; Tsui, V.; Wan, N. C.; Wang, S. M.; Wong, S.; Zhu, B. Y. *Bioorg. Med. Chem. Lett.* **2010**, *20*, 2408.
4. Folkes, A. J.; Ahmadi, K.; Alderton, W. K.; Aliz, S.; Baker, S. J.; Box, G.; Chuckowree, I. S.; Clarke, P. A.; Depledge, P.; Eccles, S. A.; Friedman, L. S.; Hayes, A.; Hancox, T. C.; Kugendradas, A.; Lensun, L.; Moore, P.; Olivero, A. G.; Pang, J.; Patel, S.; Pergl-Wilson, G.; Raynaud, F. I.; Robson, A.; Saghir, N.; Salphati, L.; Sohal, S.; Ultsch, M. H.; Valenti, M.; Wallweber, H. J. A.; Wan, N. C.; Wiesmann, C.; Workman, P.; Zhyvoloup, A.; Zvelebil, M. J.; Shuttleworth, S. J. *J. Med. Chem.* **2008**, *51*, 5522.
5. Enzymatic activity of the PI3K isoforms was measured using a competitive displacement fluorescence polarization assay as described previously (Sutherlin et al.).[2] All IC_{50}s reported are geometric means of at least duplicate measurements. Anti-proliferative activity in the MCF7.1 cell line was measured following a 3-day incubation using Cell-titer Glo™. The MCF7.1 cell line is an in vivo selected line developed at Genentech and originally derived from the parental human MCF7 breast cancer cell line (ATCC, Manassas, VA). IC_{50}s were determined using a 4-parameter fit and are geometric means of multiply replicates.
6. *c* Log *P* determined using biobyte® software. LE = ligand efficiency = $\Delta G/N_{non\text{-}hydrogen\ atoms}$; lipE = lipophilic efficiency = pIC_{50} (PI3Kα) − *c* Log *P*.
7. The halogen does not have clear density in these structures, however, modeling suggests it occupies this hydrophobic pocket (**1f** and **6**).
8. 8 of 9 *N*-methylaniline amides in the Cambridge structural database display a 'cis' conformation (most containing ortho halogens). 8 of 17 *N*-methyl-*N*-isopropyl amides are in the 'trans' orientation. For discussion of solid-state structures of *N*-methylaniline amides see: (a) Itai, A.; Toriumi, Y.; Saito, S.; Kagechika, H.; Shudo, K. *J. Am. Chem. Soc.* **1992**, *114*, 10649; (b) Toriumi, Y.;

Kasuya, A.; Itai, A. *J. Org. Chem.* **1990**, *55*, 259; (c) Kagechika, H.; Himi, T.; Namakawa, K.; Kawachi, E.; Hashimoto, Y.; Shudo, K. *J. Med. Chem.* **1989**, *32*, 2292. and references therein.
9. For a detailed description of synthetic work related to this manuscript please see: Do, S.; Goldsmith, R.; Heffron, T.; Kolesnikov, A.; Staben, S.; Olivero, A.; Siu, M.; Sutherlin, D. P.; Zhu, B.-Y.; Goldsmith, P.; Bayliss, T.; Folkes, A.; Pegg, N. WO/2009/123971.
10. We also saw a qualitative improvement in chemical stability as benzopyran analogs often decomposed after prolonged storage in DMSO.
11. Leeson, P. D.; Springthorpe, B. *Nat. Rev. Drug Disc.* **2007**, *6*, 881; For an example of a lead optimization program analyzed by progressive lipE optimization see: Ryckmans, T.; Edwards, M. P.; Horne, V. A.; Correia, A. M.; Owen, D. R.; Thompson, L. R.; Tran, I.; Tutt, M. F.; Young, T. *Bioorg. Med. Chem. Lett.* **2009**, *19*, 4406.
12. Metasite® metabolism prediction software predicted *N*-de-methylation and para-aniline-oxidation of **4** to be major oxidative metabolites.
13. Cryopreserved human hepatocytes, $[\mathbf{11}]_i = 5\ \mu M$. The major metabolite by UV 254 was identified to be the amide hydrolysis product.
14. For information regarding reactivity and potential toxicity of metabolites of anilines see: (a) Blagg, J. *Annal. Rep. Med. Chem.* **2006**, *41*, 353; (b) Hop, E. C. A.; Kalgutkar, A. S.; Soglia, J. R. *Annal. Rep. Med. Chem.* **2006**, *41*, 370; (c) Kalgutkar, A. S.; Dalvia, D. K.; O'Donnell, J. P.; Taylor, T. J.; Sahakian, D. C. *Curr. Drug Met.* **2002**, *3*, 379.
15. The delay in pathway knockdown for **15** versus GDC-0941 is likely due to different rates of absorption. **15** dosed at 50 mg/kg in MCT vehicle in nude mice had a $T_{max} \sim 3$ h. GDC-0941 dosed at 50 mg/kg in MCT vehicle in nude mice had a T_{max} <30 min. MTD for **15** was not determined in this study.
16. Heffron et al. in preparation.